Applied Mathematics and Computation 218 (2012) 11842–11850

Contents lists available at SciVerse ScienceDirect

Applied Mathematics and Computation

journal homepage: www.elsevier.com/locate/amc

Quasi wavelet based numerical method for a class of partial integro-differential equation ☆

Wenting Long [a], Da Xu [b,*], Xueying Zeng [c]

[a] School of Mathematics and Computational Science, Sun Yat-sen University, Guangzhou 510275, PR China
[b] College of Mathematics and Computer Science, Hunan Normal University, Changsha 410081, PR China
[c] School of Mathematical Sciences, Ocean University of China, Qingdao 266100, PR China

ARTICLE INFO

Keywords:
Partial integro-differential equation
Quasi-wavelets
Forward Euler method
Regularization
Numerical method

ABSTRACT

In this paper we study the numerical solution of initial-boundary problem for a class of partial integro-differential equations. The quasi wavelet method is proposed to handle the spatial derivatives while the forward Euler method is used to discretize the temporal derivatives. Detailed discrete schemes are given and some numerical experiments are included to demonstrate the effectiveness of the discrete technique. The comparisons of the present numerical results with the exact analytical solutions show that the quasi wavelet based numerical method has distinctive local property and can achieve accurate results.

1. Introduction

In this paper we consider quasi-wavelet based numerical method for a class of partial integro-differential equations having the form of

$$u_t(x,t) = \int_0^t \beta(t-s)\Delta u(x,s)ds + f(x,t), \quad x \in \Omega,\ 0 < t \leqslant T \tag{1.1}$$

along with the boundary condition

$$u(x,t) = 0, \quad (x,t) \in \partial\Omega \times [0,T] \tag{1.2}$$

and the initial condition

$$u(x,0) = v(x), \quad x \in \Omega, \tag{1.3}$$

where Δ and $\partial\Omega$ denote the two-dimensional Laplace operator and the boundary of Ω, respectively. This type of equations often arises from the applications such as heat conduction in materials with memory, biological models and chemical kinetics, compression of visco-elastic media, fluid dynamics and nuclear reactor dynamics.

Since analytical solution can only be available to a few limited cases, computer simulation is the major approach for the integro-differential equation appearing in Eq. (1.1). To achieve this goal, many methods have been employed for numerically treating the integro-differential equations. These methods include finite-element methods [1–13], finite-difference methods [14,15], orthogonal spline collocation methods [16,17], spectral collocation methods [18] and Galerkin methods [19].

☆ Project supported by the National Nature Science Foundation of China (Nos. 10271046, 10971062).
* Corresponding author.
E-mail addresses: longwenting@gmail.com (W. Long), daxu@hunnu.edu.cn (D. Xu), auwizeng@gmail.com (X. Zeng).

0096-3003/$ - see front matter © 2012 Elsevier Inc. All rights reserved.
http://dx.doi.org/10.1016/j.amc.2012.04.090

However, due to the possible singularities of the kernel β which will induce sharp transitions in the solution, developing accurate numerical methods for integro-differential equations is still a challenge. Wavelets-based method is an effective way in handling the sharp transitions caused by the singularities of the kernel. This is because the localization properties make the wavelets have good ability to analyze the local characteristics of functions. The wavelets can be expressed as a superposition of its orthonormal scaling function [20]. Wei in [21] proposed the quasi wavelets by regularizing the orthogonal scaling functions. Quasi wavelets have much better local properties than its original wavelets, which is of particular importance for numerically resolving sharp transition in the solutions for integro-differential equations. This motivates us to propose the quasi wavelets based numerical methods for integro-differential equations in this paper.

The organization of this paper is as follows. In Section 2, we give a brief introduction to the quasi-wavelets theory. Based on quasi-wavelets, we develop the fully discrete scheme and numerical algorithms for partial integro-differential equation in Section 3. The numerical experiments confirming the efficiency of the proposed method are presented in Section 4. This paper ends with a conclusion.

2. Quasi wavelet based numerical method

This section includes two subsections. In the first subsection, we give a brief introduction to quasi wavelet theory. Quasi wavelet was proposed in [22] and has good ability in characterizing the localized variations of functions. The second subsection is devoted to the quasi wavelet based numerical scheme.

2.1. Introduction to quasi wavelet

As is well known, a wavelet system can construct an orthonormal basis for $L^2(\mathbb{R})$. This system is generated from a single mother wavelet function $\psi(x)$, by standard operations of dilation and translation

$$\psi_{\alpha,\beta}(x) := \alpha^{-\frac{1}{2}}\psi\left(\frac{x-\beta}{\alpha}\right),$$

where α and β are dilation and translation factors, respectively. The wavelet function $\psi(x)$ can be constructed by its corresponding orthonormal scaling function $\phi(x)$. There are many orthonormal scaling functions in the literature, among which we are interested in the delta sequence kernel of Dirichlet type [23]. This type of scaling functions has the form of

$$\phi(x) := \delta_\alpha(x) := \frac{1}{\pi}\int_0^\alpha \cos(xy)dy = \frac{\sin(\alpha x)}{\pi x}. \tag{2.1}$$

An important example is the Shannon scaling function when $\alpha = \pi$ in Eq. (2.1). Shannon scaling function has been widely used in many research fields such as mathematics, signal processing and information theory.

The Dirichlet's delta sequence kernel provides a basis for the Paley–Wiener reproducing kernel Hilbert space B_α^2, which is a subspace of $L^2(\mathbb{R})$. Therefore, a function $f(x)$ whose Fourier transform $\widehat{f}(\omega)$ is supported on the interval $[-\alpha,\alpha]$, that is $f \in B_\alpha^2$, can be exactly reproduced as

$$f(x) = \int_{-\infty}^{+\infty} \delta_\alpha(x-y)f(y)dy. \tag{2.2}$$

There is a useful sampling scaling function in the Paley–Wiener reproducing kernel Hilbert space B_α^2

$$\delta_{\alpha,k} = \delta_\alpha(x-x_k) = \frac{\sin(\alpha(x-x_k))}{\pi(x-x_k)}, \tag{2.3}$$

where $\{x_k\}$ is the set of sampling points. By equations in (2.2) and (2.3), we can represent every function $f(x)$ in B_α^2 in the discrete form

$$f(x) = \sum_{k=-\infty}^{+\infty} \delta_\alpha(x-x_k)f(x_k). \tag{2.4}$$

To use the sampling scaling function $\delta_\alpha(x-x_k)$ in Eq. (2.4), we should select a suitable value for the parameter α. The Shannon sampling theorem asserts that, for a given bandlimited signal in B_α^2, the uniformly spatial discrete samples can completely represent it if we sample at the Nyquist frequency $\alpha = \frac{\pi}{\Delta}$, where Δ is the spatial grid size. With $\alpha = \frac{\pi}{\Delta}$, we have

$$f(x) = \sum_{k=-\infty}^{+\infty} \delta_\alpha(x-x_k)f(x_k) = \sum_{k=-\infty}^{+\infty} \frac{\sin[\pi(x-x_k)/\Delta]}{\pi(x-x_k)/\Delta} f(x_k). \tag{2.5}$$

However, the Fourier transform of $\delta_\alpha(x)$ is discontinuous, $\delta_\alpha(x)$ and $\delta_{\alpha,k}(x)$ have therefore no significant local property in spatial domain. To improve the localized and asympotic behavior of Dirichlet's delta sequence kernel, Wei et al. [24] proposed to increase its regularity by introducing a regularizer $R_\sigma(x)$. The regularized scaling function has the form of

$$\delta_{\alpha,\sigma}(x) := \delta_\alpha(x)R_\sigma(x), \tag{2.6}$$

where the regularizer $R_\sigma(x)$ satisfies

$$\lim_{\sigma\to\infty} R_\sigma(x) = 1$$

and

$$\int_{-\infty}^{+\infty} \lim_{\sigma\to\infty} \delta_\alpha(x)R_\sigma(x)dx = R_\sigma(0) = 1.$$

An immediate benefit of the regularized scaling function is its good localization ability due to the continuousness of its Fourier transform. Among the regularizers satisfying above two conditions, we choose the Gaussian type regularizer [25]

$$R_\sigma(x) = \exp(-\frac{x^2}{2\sigma^2}), \quad \sigma > 0, \tag{2.7}$$

where σ denotes the width parameter. In this paper, we set $\sigma = r\cdot\Delta$, where r is determined in numerical computation and usually has the range of $[1.8, 3.5]$. Using the Gaussian regularizer $R_\sigma(x)$, the resulting Gaussian regularized scaling function is

$$\delta_{\Delta,\sigma}(x) = \frac{\sin(\pi x/\Delta)}{\pi x/\Delta}\exp\left(-\frac{x^2}{2\sigma^2}\right). \tag{2.8}$$

The regularized shannon kernel $\delta_{\Delta,\sigma}(x)$ has better localization property than the original shannon kernel because of the continuity of its Fourier transform. However, the function $\delta_{\Delta,\sigma}(x)$ is no more exact orthonormal wavelet scaling function. It was called quasi scaling function in [25]. The wavelet generated by quasi scaling function is called quasi wavelet. Since quasi wavelet method is actually a kind of finite differential method and approximates to spectral method which possesses global accuracy and local flexibility for both linear and nonlinear systems [24], we consider to use it to solve the integro differential we have mentioned above.

2.2. Quasi wavelet based numerical scheme

Using the quasi scaling function $\delta_{\Delta,\sigma}(x)$, the function f in B_α^2 can be represented as

$$f(x) = \sum_{k=-\infty}^{+\infty} \delta_{\Delta,\sigma}(x-x_k)f(x_k) = \sum_{k=-\infty}^{+\infty} \delta_\alpha(x-x_k)R_\sigma(x-x_k)f(x_k). \tag{2.9}$$

It is obviously that the requirement of infinite sampling points is impractical for numerical computation. However, since the Gaussian regularizer in Eq. (2.7) has rapid decay behavior, we only need to select those sampling points close to x when compute the value of $f(x)$. Therefore, the Eq. (2.9) can be simplified as

$$f(x) = \sum_{k=-W}^{W} \delta_{\Delta,\sigma}(x-x_k)f(x_k) \tag{2.10}$$

and the n-th order derivatives of $f(x)$ can be computed as

$$f^{(n)}(x) = \sum_{k=-W}^{W} \delta_{\Delta,\sigma}^{(n)}(x-x_k)f(x_k), \quad n = 1, 2, \tag{2.11}$$

where $2W+1$ is the computational bandwidth centering around x. As it can be seen from Eqs. (2.10) and (2.11), the value of a function and its derivatives at a point x are approximated by the weighted sum of the function values at $2W$ neighboring points and the point x. Therefore, they can preserve the local features of the function f. We call the schemes in Eqs. (2.10) and (2.11) the quasi wavelet based numerical schemes.

It is obviously that $f(x_k)$ may locate outside of the computational domain $[a, b]$. In this case, $f(x_k)$ can usually be determined according to corresponding boundary conditions [25].

(1) For Dirichlet boundary condition, $f(x_k) = f(a)$ or $f(b)$.
(2) For periodic boundary condition, $f(x_k)$ is gotten by periodic mapping from their corresponding values inside the computational domain $[a, b]$.
(3) For Neumann boundary condition, $f(x_k)$ is determined by $f(a)$ (or $f(b)$).

The derivative terms $\delta_{\Delta,\sigma}^{(n)}(x-x_k)$ appearing in Eq. (2.11) are given by

$$\delta_{\Delta,\sigma}^{(n)}(x-x_k) = \frac{\mathrm{d}^n}{\mathrm{d}x^n}\delta_{\Delta,\sigma}(x-x_k), \quad n = 1, 2.$$

For the computational convenience, we give the detailed formulas of $\delta_{\Delta,\sigma}^1(x)$ and $\delta_{\Delta,\sigma}^2(x)$ as follows

$$\delta^{(1)}_{\Delta,\sigma}(x)=\begin{cases}-\frac{\cos(\pi x/\Delta)}{x}\exp\left(-\frac{x^2}{2\sigma^2}\right)-\frac{\sin(\pi x/\Delta)}{\pi x^2/\Delta}\exp\left(-\frac{x^2}{2\sigma^2}\right)\\ -\frac{\sin(\pi x/\Delta)}{\pi\sigma^2/\Delta}\exp\left(-\frac{x^2}{2\sigma^2}\right), & (x\neq 0)\\ 0. & (x=0)\end{cases} \tag{2.12}$$

$$\delta^{(2)}_{\Delta,\sigma}(x)=\begin{cases}-\frac{\sin(\pi x/\Delta)}{x\Delta/\pi}\exp\left(-\frac{x^2}{2\sigma^2}\right)-2\frac{\cos(\pi x/\Delta)}{x^2}\exp\left(-\frac{x^2}{2\sigma^2}\right)\\ -2\frac{\cos(\pi x/\Delta)}{\sigma^2}\exp\left(-\frac{x^2}{2\sigma^2}\right)+2\frac{\sin(\pi x/\Delta)}{\pi x^3/\Delta}\exp\left(-\frac{x^2}{2\sigma^2}\right)\\ +\frac{\sin(\pi x/\Delta)}{x\pi\sigma^2/\Delta}\exp\left(-\frac{x^2}{2\sigma^2}\right)+x\frac{\sin(\pi x/\Delta)}{\pi\sigma^4/\Delta}\exp\left(-\frac{x^2}{2\sigma^2}\right), & (x\neq 0)\\ -\frac{3+\pi^2\sigma^2/\Delta^2}{3\sigma^2}. & (x=0)\end{cases} \tag{2.13}$$

3. Proposed algorithms

In this section, we propose the quasi wavelet based numerical algorithms for solving the one dimensional partial integro-differential equations with the kernel $\beta(s,t)=(t-s)^{-\eta}$, i.e.

$$u_t(x,t)=\int_0^t(t-s)^{-\eta}u_{xx}(x,s)ds+f(x,t),\quad 0<x<1,\ 0<t\leqslant T \tag{3.1}$$

along with the boundary condition

$$u(0,t)=u(1,t)=0,\quad 0<t\leqslant T \tag{3.2}$$

and the initial condition

$$u(x,0)=v(x),\quad 0<x<1. \tag{3.3}$$

The kernel $(t-s)^{-\eta}$ has weak singularity when $0<\eta<1$. First, we present a detailed description of spatial–temporal discretization about this type of equation. A quasi wavelet based numerical algorithm is then described for solving the considered equation.

3.1. Discretization in time: a forward Euler scheme

We discretize the time-derivative in Eq. (3.1) by the first order forward Euler scheme. Let $t_n=n\triangle t$ with $\triangle t$ being the time step. Let u^n be the approximation to the value of $u(t,x)$ at the time point $t=t_n,\ n=0,1,\ldots,N,\ N=[T/K]$. Considering the temporal discrete process of Eq. (3.1) at time point $t=t_n$, the left side of the equation can be approximated by

$$u_t(x,t_n)\approx(\triangle t)^{-1}(u^{n+1}(x)-u^n(x)),\quad 0<x<1,\ n\geqslant 0 \tag{3.4}$$

and the second term, $(t-s)^{-\eta}\Delta u(x,s)$, can be approximated by

$$\begin{aligned}\int_0^{t_n}(t_n-s)^{-\eta}u_{xx}(x,s)ds&\approx\sum_{l=0}^{n-1}\int_{t_l}^{t_{l+1}}(t_n-s)^{-\eta}u_{xx}(x,s)ds\approx\sum_{l=0}^{n-1}u^l_{xx}(x)\int_{t_l}^{t_{l+1}}(t_n-s)^{-\eta}ds\\&=\sum_{l=0}^{n-1}u^l_{xx}(x)\frac{(\triangle t)^{1-\eta}}{\eta-1}[(n-l-1)^{1-\eta}-(n-l)^{1-\eta}],\quad 0<x<1,\ n\geqslant 1.\end{aligned} \tag{3.5}$$

For convenience, we introduce the following notations: $\rho_l:=[(n-l-1)^{1-\eta}-(n-l)^{1-\eta}],\ l=0,1,\ldots,n-1$, and $Q=(\triangle t)^{1-\eta}/(\eta-1)$. Substituting Eqs. (3.4) and (3.5) into Eq. (3.1), we can get the temporal semi-discrete form of Eq. (3.1)

$$u^{n+1}(x)=u^n(x)+\triangle t\left(f^n(x)-Q\sum_{l=0}^{n-1}u^l_{xx}(x)\rho_l\right),\quad 0<x<1,\ n\geqslant 1. \tag{3.6}$$

For the special case $n=0$, which is the first time step, the scheme simply reads

$$u^1=u^0+\triangle t f^0(x),\quad 0<x<1,\ n=0. \tag{3.7}$$

3.2. Discretization in space: quasi wavelet based numerical method

We discretize the spatial-derivative by the described quasi wavelet based numerical method in Section 2. We consider the uniform grid

$$0=x_0<x_1<\cdots<x_I=1.$$

Let $\triangle x=\frac{1}{I}$ denote the spatial step. We denote a grid point (x_i,t_n) by $t_n=n\triangle t,\ x_i=i\triangle x$, u^n_i is an approximation to the value of $u(x,t)$ at the grid point (x_i,t_n) with $n\geqslant 0,\ i=0,1,\ldots,I$. We can use Eq. (2.11) to discretize the spatial derivatives. The quasi

wavelet based numerical method told us that, due to the rapid decay of the Gaussian weight, only $2W$ grid points x_i, which are the near "neighbor gird" points to x, need be included in the sum. For example, the value of the j-th order derivative $u_x^{(j)}(x,t)$ at the grid point (x_i,t_n) $(n \geqslant 0,\ 1 \leqslant i \leqslant I)$ is approximated by

$$u_x^{(j)}(x_i,t_n) = \sum_{k=i-W}^{i+W} \delta_{\Delta,\sigma}^{(j)}(x_i - x_k)u(x_k,t_n), \quad j = 0,1,2. \tag{3.8}$$

Substituting Eq. (3.8) into Eq. (3.6) and setting $x = x_i$, for $n = 0,1,\ldots,N,\ i = 0,1,\ldots,I$, we have

$$u^{n+1}(x_i) = u^n(x_i) + \triangle t\left(f^n(x_i) - Q\sum_{l=0}^{n-1}\sum_{k=i-W}^{i+W} \delta_{\Delta,\sigma}^{(2)}(x_i - x_k)u^n(x_k)\rho_l\right)$$

Remembering that u_i^n denotes the value of $u(x,t)$ at the grip point (x_i,t_n), the above equation can be rewritten as

$$u_i^{n+1} = u_i^n + \frac{1}{2}(\triangle t)^3\sum_{l=0}^{n-1}\sum_{k=i-W}^{i+W}(2n-2l+1)u_{k+i}^l\delta_{\Delta,\sigma}^{(2)}(\triangle t\Delta x) + \triangle t f_i^n, \tag{3.9}$$

where

$$u_i^1 = u_i^0 + \triangle t f_i^0, \quad i = 0,1,\ldots,I$$

and

$$u_0^n = u_1^n = 0, n = 0,1,\ldots,N.$$

Since function values of $u(x,t)$ are usually undefined outside the spatial domain $[0,1]$ and the boundary condition is assumed to be Dirichlet type, we extend our zero boundary condition and setting

$$u_k^n = 0, \quad k < 0, \quad or \quad k > I,\ n = 0,1,2,\ldots N.$$

In addition, the initial condition $u(x,0) = v(x)$ can be easily discretized as

$$u_i^0 = v(x_i), \quad i = 0,1,\ldots,I.$$

4. Numerical experiments

In this section we present the numerical experiments of the proposed methods. All computations below are carried out on a PC equipped with Core Duo and 1.5 G RAM and Matlab R2007a. For simplicity, a uniform grid is considered.

NOTES: k must be small enough. On the one hand, by choosing small time step we can attribute most of the errors to the spatial discretization; On the other hand, it has been proved that the truncation error of the algorithm using the regularized Shannon's kernel decays exponentially when the spatial sampling point increases [26]. The parameter r is chosen between 2.2 and 4.0 to generate good results. We also find out that we only need to take $2W$ $(W \geqslant 35)$ sampling points in the vicinity of x to get high computational accuracy [25]. How to choose the values of W,δ and σ? Qian and Wei [27] have presented a mathematical estimation of approximation errors. Their results provide a guide for the choice which is in excellent agreement with an earlier numerical test [21]. And the factors $\delta_{\Delta,\sigma}^{(1)}, \delta_{\Delta,\sigma}^{(2)}$ have been given in Eqs. (2.12) and (2.13).

We denote computational solution and exact analytical solution by u and v, respectively. The L_∞ error estimation is given by

$$L_\infty = \max|u_i - v_i|_{i=0}^{i=N} \Big/ |v_i|. \tag{4.1}$$

Example 1. Let us consider the problem

$$u_t(x,t) - \int_0^t (t-s)u_{xx}(x,s)ds = f(x,t), \quad 0 < x < 1,\ 0 < t \leqslant T, \tag{4.2}$$

$$u(0,t) = u(1,t) = 0. \tag{4.3}$$

along with the initial conditions $u(x,0) = x(1-x)$. In the case of

$$f(x,t) = \left(4 + \frac{3}{2}x - \frac{3}{2}x^2\right)t^{1/2} + 4t^2. \tag{4.4}$$

the exact analytical solution can be given by $u(x,t) = x(1-x)(t^{3/2}+1)$.

We set $T = 1$ for numerical consideration. In Table 1, we show the results of the 50th, 150th, 250th, 350th, 450th time points at two different grid sizes, k = 0.00001 s and k = 0.000001 s. We can conclude that:

Table 1
L_∞ of Example 1.

$\Delta t = 0.00001$				$\Delta t = 0.000001$			
J	r	W	L_∞	J	r	W	L_∞
10	3	7	7.6355e−010	10	3	7	7.6370e−013
			2.0534e−008				2.0555e−011
			9.4921e−008				9.5080e−011
			2.6018e−007				2.6079e−010
			5.5245e−007				5.5412e−010
20	3	7	2.4556e−009	20	3	7	2.3141e−012
			6.4036e−008				6.2835e−011
			2.9420e−007				2.9119e−010
			8.0428e−007				7.9931e−010
			1.7053e−006				1.6991e−009
20	2	7	2.9482e−009	20	2	7	2.7776e−012
			7.7067e−008				7.5620e−011
			3.5424e−007				3.5061e−010
			9.6863e−007				9.6264e−010
			2.0540e−006				2.0465e−009
20	3	15	2.6875e−009	20	3	15	2.7851e−012
			7.0171e−008				7.5804e−011
			3.2246e−007				3.5147e−010
			8.8165e−007				9.6499e−010
			1.8694e−006				2.0516e−009

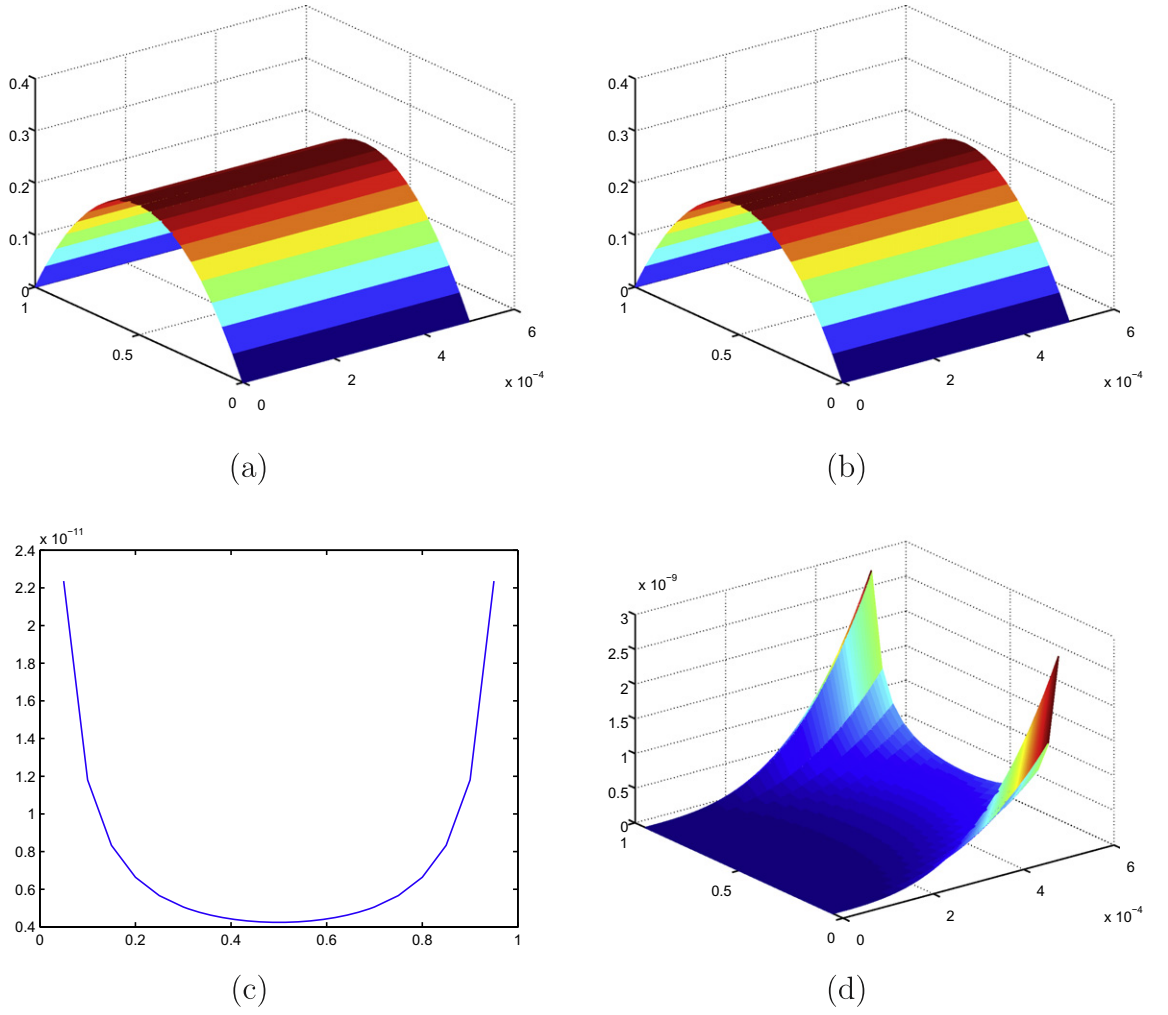

Fig. 1. One result when $J = 20$, $M = 500$, $r = 3$, $w = 7$, $k = 0.00001$, $q = 100$. (a) The computational solution u, (b) the analytical solution v, (c) L_∞ error estimation at the time point and (d) the global L_∞ error estimation.

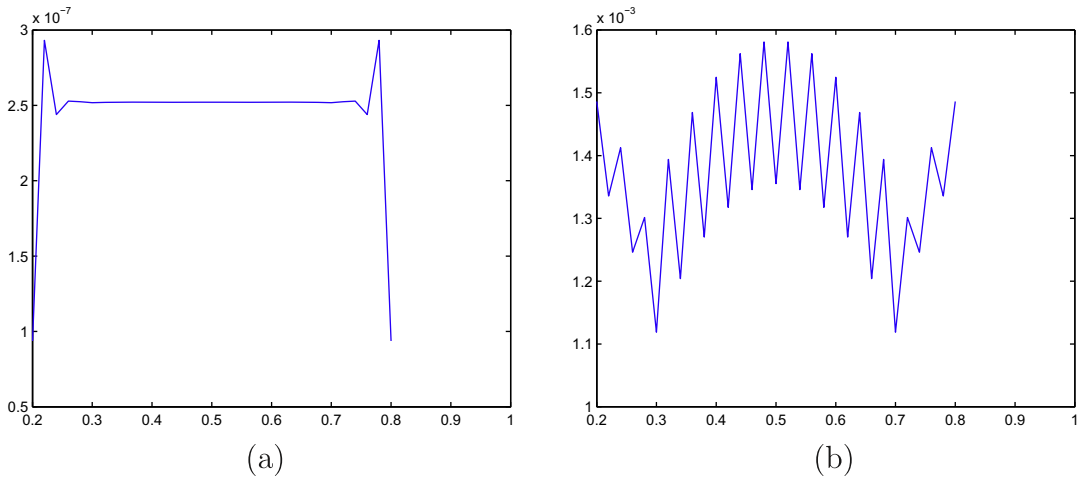

Fig. 2. The error between the computational and analytical solutions (a) without the regularizer and (b) with the regularizer.

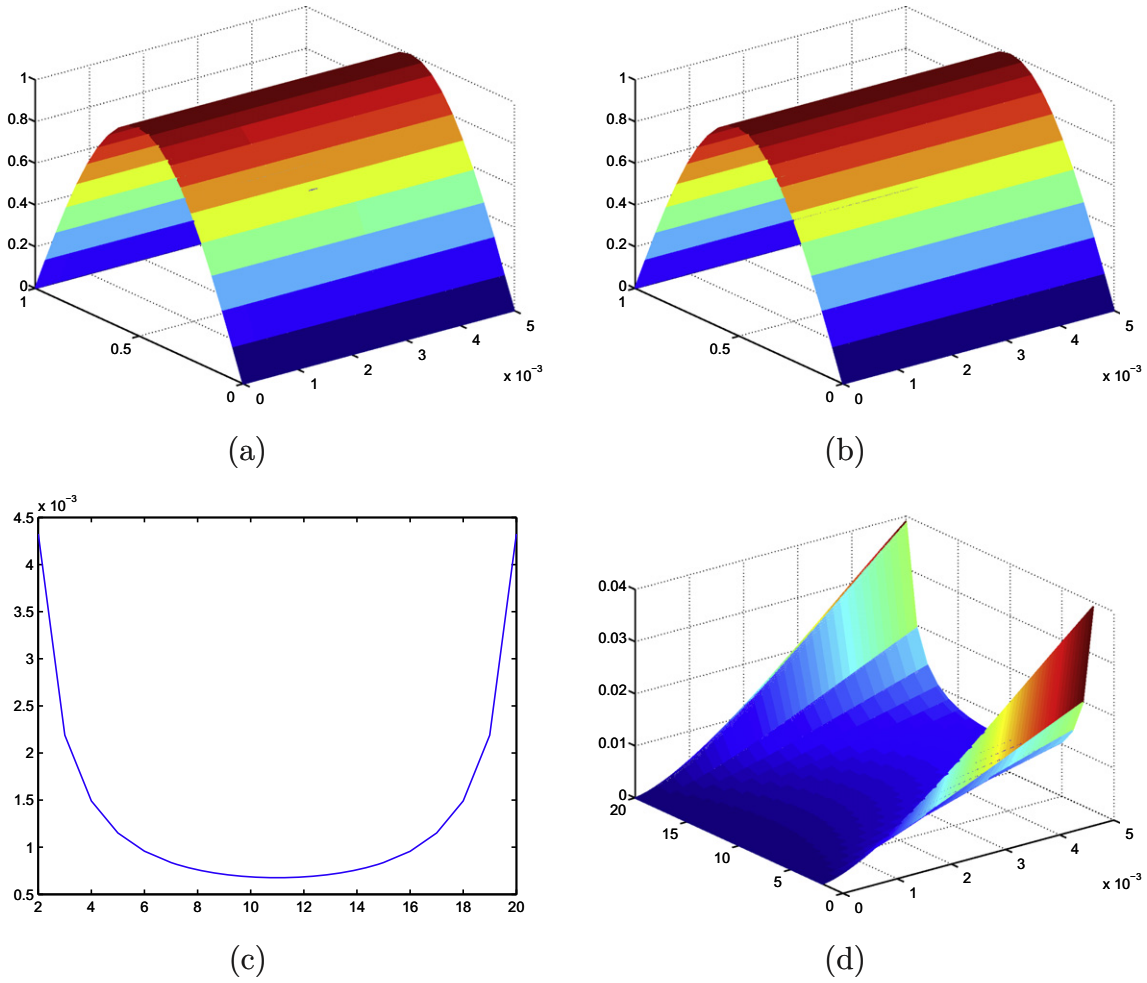

Fig. 3. One result when $J = 20,\ M = 500,\ r = 3,\ W = 7,\ k = 0.00001$ s, $t = 0.001$ s. (a) The computational solution u, (b) the analytical solution v, (c) L_∞ error estimation at the time point and (d) the global L_∞ error estimation.

Table 2
L_∞ of Example 3.

$\Delta t = 0.00001$				$\Delta t = 0.000001$			
J	r	W	L_∞	J	r	W	L_∞
10	3	7	4.9343e−004	10	3	7	1.5630e−005
			2.5228e−003				8.0470e−005
			5.3616e−003				1.7272e−004
			8.7631e−003				2.8572e−004
			1.2588e−002				4.1611e−004
20	3	7	1.5825e−003	20	3	7	5.0435e−005
			7.8974e−003				2.6001e−004
			1.6182e−002				5.5766e−004
			2.5304e−002				9.2134e−004
			3.4578e−002				1.3397e−003
20	2	7	1.9477e−003	20	2	7	6.2048e−005
			2.0001e−002				3.1995e−004
			3.1373e−002				6.8631e−004
			9.6863e−007				1.1340e−003
			4.3029e−002				1.6491e−003
20	3	15	1.7790e−003	20	3	15	5.6664e−005
			8.8998e−003				2.9217e−004
			1.8299e−002				6.2673e−004
			2.8739e−002				1.0356e−003
			3.9473e−002				1.5061e−003

(1) Quasi-wavelet method has very high accuracy. When k = 0.000001 s, $L_\infty = 7.6370\text{e}{-013}$.
(2) When the time step increases an order of magnitude, L_∞ increases three orders of magnitude, which means that the error is mainly communicated in time direction.
(3) L_∞ does not reduce with the reduction of r, This is consistent with what we said above.

At the same time, we plot the result of $J = 20,\ k = 0.00001$ s, $r = 3,\ W = 7,\ t = 0.001$ s in Fig. 1. We can also see that the computational solution u is highly consistent with the analytical solution v, which shows the wavelet method is very effective. The Fig. 1-(d) shows the error evolution with time. In practical simulations, the parameters r and W are selected to achieve good results.

Example 2. We also show the error between the computational and analytical solutions of Eq. (4.2) at $J = 50,\ r = 3,\ W = 7,\ k = 0.000001$ s, $t = 0.0005$ s. Fig. 2-(a) shows this error when we do not use the regularizer $R_\sigma(x)$ in quasi-wavelet method. The error of introducing the regularizer $R_\sigma(x)$ is shown in Fig. 2-(b). We can clearly conclude that the computational solution obtained by using $R_\sigma(x)$ is more close to the analytical solution.

Example 3. We then test the performance of the proposed method in solving the partial integro-differential equation with weak singular kernel:

$$u_t(x,t) - \int_0^t (t-s)^{-1/2} u_{xx}(x,s)ds = f(x,t), \quad 0 < x < 1,\ 0 < t \leqslant T, \tag{4.5}$$

$$u(0,t) = u(1,t) = 0 \tag{4.6}$$

along with the initial conditions $u(x,0) = \sin(\pi x)$. In the case of

$$f(x,t) = \frac{2t^{1/2}}{\sqrt{\pi}}(\pi^2 \sin \pi x - \sin 2\pi x) - 2\pi^2 t^2 \sin 2\pi x, \tag{4.7}$$

the exact analytical solution is given by $u(x,t) = \sin \pi x - \frac{4t^{3/2}}{3\sqrt{\pi}} \sin 2\pi x$.

We set $T = 1$ for numerical consideration. In Table 2, we show the results of the 50th, 150th, 250th, 350th, 450th time points of the two different grid sizes, $k = 0.00001$ s and $k = 0.000001$ s. About r and W, we can get the same conclusion with Example 1.

We show the results of $J = 20,\ M = 500,\ r = 3,\ W = 7,\ k = 0.00001$ s, $t = 0.001$ s in Fig. 3, and we can see again the result is also accurate. By comparing the result of Example 1 and 3, we can find that the results have several orders of magnitude difference. In addition, in Example 3, the error estimate changes little when the time step becomes smaller. This is mainly because the equation is singular at $t = 0$.

5. Conclusions

The quasi wavelet based numerical method has been used for solving the partial integro differential equations in this paper. In the computing process, the forward Euler method was used to discretize the temporal derivatives while the quasi wavelet method was adopted to handle the spatial derivatives. We have shown that the numerical results have high accuracy comparing with the analytical results. This demonstrates that the present numerical method has the ability to effectively resolve such equations.

References

[1] C. Chen, V. Thomée, L. Wahlbin, Finite element approximation of a parabolic integro-differential equation with a weakly singular kernel, Math. Comput. 58 (1992) 587–602.
[2] W. McLean, V. Thomée, Numerical solution of an evolution equation with a positive-type memory term, J. Aust. Math. Soc. Ser. B 35 (1993) 23–70.
[3] I. Sloan, V. Thomée, Time discretization of an integro-differential equation of parabolic type, SIAM J. Numer. Anal. (1986) 1052–1061.
[4] S. Larsson, V. Thomée, L. Wahlbin, Numerical solution of parabolic integro-differential equations by the discontinuous Galerkin method, Math. Comput. 67 (1998) 45–71.
[5] W. McLean, V. Thomée, L. Wahlbin, Discretization with variable time steps of an evolution equation with a positive-type memory term, J. Comput. Appl. Math. 69 (1996) 49–69.
[6] C. Lubich, Discretized fractional calculus, SIAM J. Math. Anal. 17 (1986) 704.
[7] E. Yanik, G. Fairweather, Finite element methods for parabolic and hyperbolic partial integro-differential equations, Non-Linear Anal. 12 (1988) 809.
[8] Y. Huang, Time discretization scheme for an integro-differential equation of parabolic type, J. Comput. Math. 12 (1994) 259–263.
[9] D. Xu, The long-time global behavior of time discretization for fractional order Volterra equations, Calcolo 35 (1998) 93–116.
[10] D. Xu, The global behavior of time discretization for an abstract Volterra equation in Hilbert space, Calcolo 34 (1997) 71–104.
[11] D. Xu, Non-smooth initial data error estimates with the weight norms for the linear finite element method of parabolic partial differential equations, Appl. Math. Comput. 54 (1993) 1–24.
[12] D. Xu, On the discretization in time for a parabolic integrodifferential equation with a weakly singular kernel I: smooth initial data, Appl. Math. Comput. 57 (1993) 29–60.
[13] D. Xu, On the discretization in time for a parabolic integro-differential equation with a weakly singular kernel II: nonsmooth initial data, Appl. Math. Comput. 57 (1993) 1–27.
[14] T. Tang, Superconvergence of numerical solutions to weakly singular Volterra integro-differential equations, Numer. Math. 61 (1992) 373–382.
[15] Z. Sun, X. Wu, A fully discrete difference scheme for a diffusion-wave system, Appl. Numer. Math. 56 (2006) 193–209.
[16] B. Bialecki, G. Fairweather, Orthogonal spline collocation methods for partial differential equations, J. Comput. Appl. Math. 128 (2001) 55–82.
[17] G. Fairweather, Spline collocation methods for a class of hyperbolic partial integro-differential equations, SIAM J. Numer. Anal. (1994) 444–460.
[18] Y. Lin, C. Xu, Finite difference/spectral approximations for the time-fractional diffusion equation, J. Comput. Phys. 225 (2007) 1533–1552.
[19] T. Lin, Y. Lin, M. Rao, S. Zhang, Petrov–Galerkin methods for linear Volterra integro-differential equations, SIAM J. Numer. Anal. (2001) 937–963.
[20] S. Mallat, Multiresolution approximations and wavelet orthonormal bases of $L^2(R)$, Trans. Amer. Math. Soc. 315 (1989) 69–87.
[21] G. Wei, Quasi wavelets and quasi interpolating wavelets, Chem. Phys. Lett. 296 (1998) 215–222.
[22] G. Wei, Wavelets generated by using discrete singular convolution kernels, J. Phys. A: Math. Gen. 33 (2000) 8577.
[23] G. Wei, Y. Zhao, Y. Xiang, Discrete singular convolution and its application to the analysis of plates with internal supports part 1: theory and algorithm, Int. J. Numer. Methods Eng. 55 (2002) 913–946.
[24] G. Wei, D. Zhang, D. Kouri, D. Hoffman, Lagrange distributed approximating functionals, Phys. Rev. Lett. 79 (1997) 775–779.
[25] D. Wang, G. Wei, The study of quasi wavelets based numerical method applied to Burgers' equations, Appl. Math. Mech. 21 (2000) 1099–1110.
[26] L. Qian, On the regularized Whittaker–Kotel'nikov–Shannon sampling formula, Proc. Amer. Math. Soc. 131 (2003) 1169–1176.
[27] L. Qian, G. Wei, A note on regularized Shannon sampling formulae, J. Approx. Theory (1999).